A&A 562, A120 (2014)
DOI: 10.1051/0004-6361/201322621

Astronomy & Astrophysics

Vacuum-UV spectroscopy of interstellar ice analogs

II. Absorption cross-sections of nonpolar ice molecules⋆

G. A. Cruz-Diaz[1], G. M. Muñoz Caro[1], Y.-J. Chen[2,3], and T.-S. Yih[3]

[1] Centro de Astrobiología, INTA-CSIC, Carretera de Ajalvir, km 4, Torrejón de Ardoz, 28850 Madrid, Spain
e-mail: [cruzdga;munozcg]@cab.inta-csic.es
[2] Space Sciences Center and Depeartment of Physics and Astronomy, University of Southern California, Los Angeles, CA 90089-1341, USA
[3] Department of Physics, National Central University, Jhongli City, 32054 Taoyuan Country, Taiwan

Received 6 September 2013 / Accepted 15 December 2013

ABSTRACT

Context. Dust grains in cold circumstellar regions and dark-cloud interiors at 10−20 K are covered by ice mantles. A nonthermal desorption mechanism is invoked to explain the presence of gas-phase molecules in these environments, such as the photodesorption induced by irradiation of ice due to secondary ultraviolet photons. To quantify the effects of ice photoprocessing, an estimate of the photon absorption in ice mantles is required. In a recent work, we reported the vacuum-ultraviolet (VUV) absorption cross sections of nonpolar molecules in the solid phase.
Aims. The aim was to estimate the VUV-absorption cross sections of nonpolar molecular ice components, including CH_4, CO_2, N_2, and O_2.
Methods. The column densities of the ice samples deposited at 8 K were measured in situ by infrared spectroscopy in transmittance. VUV spectra of the ice samples were collected in the 120−160 nm (10.33−7.74 eV) range using a commercial microwave-discharged hydrogen flow lamp.
Results. We found that, as expected, solid N_2 has the lowest VUV-absorption cross section, which about three orders of magnitude lower than that of other species such as O_2, which is also homonuclear. Methane (CH_4) ice presents a high absorption near Ly-α (121.6 nm) and does not absorb below 148 nm. Estimating the ice absorption cross sections is essential for models of ice photoprocessing and allows estimating the ice photodesorption rates as the number of photodesorbed molecules per absorbed photon in the ice.

Key words. astrochemistry – methods: laboratory: molecular – methods: laboratory: solid state – techniques: spectroscopic – ISM: molecules – ultraviolet: ISM

1. Introduction

Grain surface chemistry is governed by the local H/H_2 ratio. If this ratio is high, hydrogenation is the main process, H_2O is the dominant constituent, and species such as NH_3 and CH_4 are expected to form. On the other hand, if the H/H_2 ratio is substantially lower than unity, CO molecules will be abundant and species such as O_2 and N_2 are easily formed. Therefore, two types of ice mantles can be distinguished, one dominated by polar molecules and another one dominated by nonpolar, or only slightly polar, molecules (see Tielens et al. 1991; Chiar et al. 1995; Gerakines et al. 1996; Whittet et al. 1996). The relative to water abundances of CO_2 and CH_4 are between 4−44% and 0.4−8%, respectively, for the different interstellar environments (Mumma & Charnley 2011, and references therein).

Gas-phase molecular oxygen and nitrogen lack an electric dipole moment, which makes them infrared inactive. These species were therefore not detected in ice mantles and cannot be easily observed in the gas phase. In some clouds the estimated abundance of gaseous N_2 is on the order of 10^{-5} with respect to H_2 (Bergin et al. 2002), whereas the coldest and densest cores show a decrease in the gas-phase N_2 by at least a factor of two (Belloche & André 2003). O_2 has a $^3\Sigma$ ground state and thus a magnetic dipole moment enabling weak transitions in the submillimeter range between finestructure levels. Very low detection rates of O_2 were found toward Orion (Goldsmith et al. 2011) and the ρ-Oph A core (Liseau et al. 2012) with HIFI. The upper limits on O_2 and estimates of N_2 suggest relative abundances much lower than expected from the solar oxygen and nitrogen abundances. Large amounts of oxygen and nitrogen are therefore apparently missing from the gas phase and might be depleted on grains most likely in the form of O_2 and N_2 (Ehrenfreund & van Dishoeck 1998).

Synchrotron radiation has been used as a source of VUV photons to perform VUV-absorption spectroscopy of ice samples. The National Synchrotron Radiation Research Center (NSRRC) in Taiwan (Lu et al. 2005; Cheng et al. 2011; and Wu et al. 2012), ASTRID at the University of Aarhus, and the UK Daresbury Synchrotron Radiation Source (Mason et al. 2006) were used as VUV sources in their measurements. This requires application for synchrotron beamtime, leading to a limited use, and one needs to work with a transportable chamber. The use of a microwave-discharge H_2 flow UV-lamp as the source for VUV-absorption spectroscopy, employed in various astrochemistry laboratories, allows a routine performance of VUV-absorption spectroscopy in the 120−170 nm spectral range. The polar molecular components of interstellar ice were studied in Cruz-Diaz et al. (2013, Paper I). To present a more complete view of the interactions between the interstellar VUV field and icy grain mantles, we report here a similar

⋆ Data can be found at http://ghosst.osug.fr/

study on nonpolar ices. Section 2 describes the experimental protocol used in the experiments. Section 3 summarizes the VUV-absorption cross-section measurements of the different nonpolar ices studied: CO_2, CH_4, N_2, and O_2. Gas-phase VUV-absorption cross-section data adapted from other works were used for comparison with our solid-phase data. In addition, the spectra of the different species were fitted with Gaussian profiles, using an in-house IDL code, to provide an individual VUV-absorption cross section for each feature in the spectra. Sections 4 and 5 summarize the astrophysical implications and the conclusions.

2. Experimental protocol

The measurements were conducted using the Interstellar Astrochemistry Chamber (ISAC). This set-up and the standard experimental protocol were described in Muñoz Caro et al. (2010). The specific detail on the VUV-measurements of absorption cross sections of ice are provided in Paper I. ISAC mainly consists of an ultra-high-vacuum (UHV) chamber, with pressure typically in the range of $P = 3.0–4.0 \times 10^{-11}$ mbar, where an ice layer made by deposition of a gas species onto a cold finger at 8 K, achieved by means of a closed-cycle helium cryostat, can be UV-irradiated. The evolution of the solid sample was monitored with in situ transmittance FTIR spectroscopy and VUV-spectroscopy. The chemical components used for the experiments described in this paper were CO_2(gas), Praxair 99.998%; CH_4(gas), Praxair 99.999%; N_2(gas), Praxair 99.999%; and O_2(gas), Praxair 99.8%. The deposited ice layer was photoprocessed with a microwave-discharged hydrogen flow lamp (MDHL), from Opthos Instruments. The source has an UV-flux of $\approx 2 \times 10^{14}$ cm^{-2} s^{-1} at the sample position, measured by $CO_2 \rightarrow CO$ actinometry, see Muñoz Caro et al. (2010). The Evenson cavity of the lamp is refrigerated with air. The VUV-spectrum is measured routinely in situ during the irradiation experiments with the use of a McPherson 0.2 m focal length VUV monochromator (model 234/302) with a photomultiplier tube (PMT) detector equipped with a sodium salicylate window, optimized to operate from 100–500 nm (11.27–2.47 eV), with a resolution of 0.4 nm. The characterization of the MDHL spectrum was previously reported (Chen et al. 2010, Paper I) and will be discussed in more detail by Chen et al. (2013). For more details and a scheme of the experimental set-up we refer to Paper I.

3. VUV-absorption cross section of interstellar ice analogs

VUV-absorption spectra of pure ices composed of CH_4, CO_2, N_2, and O_2 have been recorded. The column density of the ice sample was measured by FTIR in transmittance. The VUV-spectrum and the column density of the ice were therefore monitored in a single experiment for the same ice sample. This improvement allowed us to estimate the VUV-absorption cross section of the ice more accurately. The column density of the deposited ice obtained by FTIR was calculated according to the formula

$$N = \frac{1}{\mathcal{A}} \int_{\text{band}} \tau_\nu \mathrm{d}\nu \quad (1)$$

where N is the column density of the ice, τ_ν the optical depth of the IR band, dν the wavenumber differential, in cm^{-1}, and $\mathcal{A}$ is the band strength in cm molecule^{-1}, see Table 1. The integrated absorbance is equal to $0.43 \times \tau$, where τ is the integrated optical depth of the IR band. The VUV-absorption cross section was estimated according to the Beer-Lambert law

$$I_t(\lambda) = I_0(\lambda) \mathrm{e}^{-\sigma(\lambda)N}$$
$$\sigma(\lambda) = -\frac{1}{N} \ln\left(\frac{I_t(\lambda)}{I_0(\lambda)}\right)$$
$$\text{with} \quad N \approx \frac{N_i + N_f}{2}, \quad (2)$$

where $I_t(\lambda)$ is the transmitted intensity for a given wavelength λ, $I_0(\lambda)$ the incident intensity, σ is the cross section in cm^2, and N is the average ice column density before (N_i) and after (N_f) exposure to VUV during VUV-spectral acquisition, in cm^{-2}. We decided to take this average value of N because the ice sample thickness decreases during exposure to VUV photons. If instead of this average value, N_i would be used as N in Eq. (2), this would lead to a lower limit of the VUV-absorption cross section. It is important to notice that the total VUV-flux value emitted by the lamp does not affect the VUV-absorption spectrum of the ice sample, since it is obtained by subtraction of two spectra to obtain the absorbance in the VUV.

Several measurements for different values of the initial ice column density were performed to improve the spectroscopy. Table 1 provides the infrared-band positions and band strengths of CH_4 and CO_2 used to estimate the column density. Solid N_2 and O_2 do not display absorption features in the mid-infrared, therefore their column densities were measured using the expression

$$N = \frac{N_A \, \rho_i \, d_i}{m_i}, \quad (3)$$

where N_A is the Avogadro constant (6.022×10^{23} mol^{-1}), ρ_i is the density of the ice in g cm^{-3}, see Table 1, m_i is the molar mass of the species in g mol^{-1}, and d_i is the ice thickness in cm. The latter was estimated following the classical interfringe relation

$$d_i = \frac{1}{2 n_i \Delta\nu}, \quad (4)$$

where n_i is the refractive index of the ice at deposition temperature, and $\Delta\nu$ is the wavenumber difference between two adjacent maxima or minima of the fringes observed in the infrared spectrum of the ice. These interference fringes are due to multiple reflections of light within the sample.

Solid O_2 was deposited at a temperature of 8 K. We used the Fulvio et al. (2009) values of n_i and ρ at 16 K as an approximation. Error values for the column density in Table 1 result mainly from the selection of the baseline for integration of the IR absorption band and the decrease of the ice column density due to

Table 1. Infrared-band positions, infrared-band strengths ($\mathcal{A}$), column density (N) in 10^{15} molec/cm^2, refractive index (n_i), and the density (ρ_i) of the samples used in this work.

Species	Position [cm^{-1}]	$\mathcal{A}$ [cm/molec^1]	N [$\times 10^{15}$ molec/cm^2]	n_i	ρ [g/cm^3]
CH_4	2343	$7.6^{+0.1}_{-0.1} \times 10^{-17}$ [a]	146^{+12}_{-29}	1.30[c]	0.47[c]
CO_2	1301	$6.4^{+0.1}_{-0.1} \times 10^{-18}$ [b]	81^{+7}_{-11}	1.21[c]	0.88[c]
N_2	–	–	4774	1.21[c]	0.94[c]
O_2	–	–	60^{+5}_{-11}	1.32[d]	1.54[d]

References. [(a)] d'Hendecourt & Allamandola (1986); [(b)] Yamada & Person (1964); [(c)] Satorre et al. (2008); [(d)] Fulvio et al. (2009).

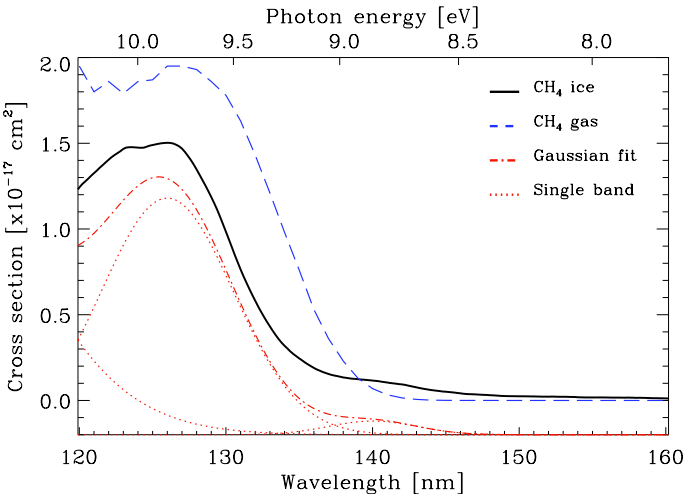

Fig. 1. VUV-absorption cross section as a function of photon wavelength (bottom X-axis) and VUV-photon energy (top X-axis) of CH_4 ice deposited at 8 K, black solid trace. The blue dashed trace is the VUV-absorption cross-section spectrum of gas phase CH_4 adapted from Lee et al. (2001). The fit of the solid-phase spectrum, red dotted (single bands, see Table 2) and dashed-dotted trace, is the sum of three Gaussians. It has been offset for clarity.

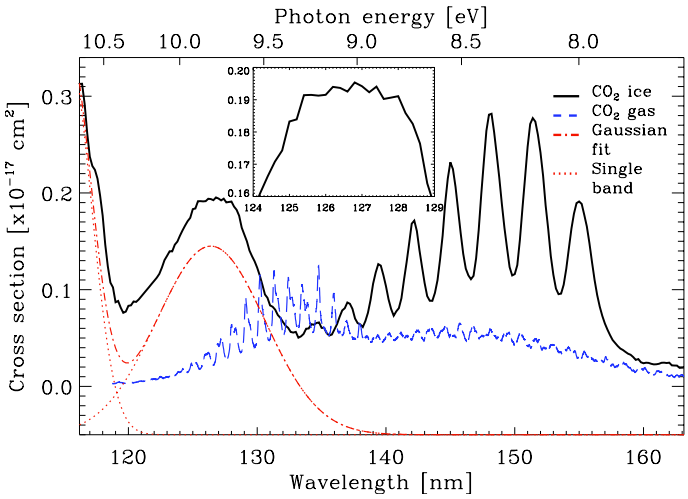

Fig. 2. VUV-absorption cross section as a function of photon wavelength (bottom X-axis) and VUV-photon energy (top X-axis) of CO_2 ice deposited at 8 K, black solid trace. The blue dashed trace is the VUV-absorption cross-section spectrum of gas phase CO_2 adapted from Yoshino et al. (1996). The fit, solid red dotted (single bands, see Table 2) and dashed-dotted trace, is the sum of two Gaussians. The *inset figure* is a CO_2 VUV-absorption cross-section close-up in the 124–129 nm range.

VUV-irradiation during spectral acquisition. The band strengths were adapted from the literature and their error estimates are no more than 10% of the reported values (Richey & Gerakines 2012). The errors in the column density determined by IR spectroscopy were 38%, 22%, and 35% for solid CH_4, CO_2, and O_2. N_2 and O_2 do not present any IR feature, but photoprocessed O_2 ice during VUV-spectral acquisition produces O_3 very readily and the loss of O_2 can be calculated. On the other hand, N_2 ice does not lead to photoproducts and the error in the column density could not be measured. The VUV-absorption cross-section errors result from the error values of the column density determination and the MDHL, photomultiplier tube (PMT), and multimeter stabilities, about 6%, using the expression

$$\delta(N) = \sqrt{\frac{\delta_i^2 + \delta_j^2 + \delta_k^2 + ... + \delta_n^2}{n-1}}. \quad (5)$$

The VUV-absorption cross-section spectra of CH_4, CO_2, N_2, and O_2 ices were fitted with Gaussian profiles using the band positions reported in the literature (Mason et al. 2006; Lu et al. 2008; Wu et al. 2012) as a starting point, see the red dotted and dashed-dotted traces in Figs. 1, 2, 4, and 5. Table 2 summarizes the Gaussian profile parameters used to fit the spectra of these ices, deposited at 8 K. Gaussian fits of the reported molecules were made with an in-house IDL code. The fits reproduce the VUV-absorption cross-section spectra well.

The main emission peaks of the MDHL occur at 121.6 nm (Lyman-α), 157.8 nm, and 160.8 nm (molecular H_2 bands). These peaks are thus also present in the secondary VUV photon spectrum generated by cosmic rays in dense interstellar clouds and circumstellar regions where molecular hydrogen is abundant (Gredel et al. 1989). For this reason, the absorption cross-section values measured at these wavelengths are provided for each molecule in the following sections. We also present an average value of the VUV-absorption cross section (a simple arithmetic mean in the spectral range indicated for each species) and an integrated VUV-absorption cross section (an integration of the form $\sigma_{\rm INT} = \int_{\lambda_i}^{\lambda_f} \sigma_\lambda d\lambda$) in the same spectral range. The same measurements were performed using the gas-phase raw data, adapted from other works, for each species.

Table 2. Parameter values used to fit the spectra of Gaussian profiles of the different molecular ices deposited at 8 K.

Molecule	Center [nm]	*FWHM* [nm]	Area [$\times 10^{-17}$ cm^2 nm]
CH_4	102.0	21.2	90.2
	126.0	10.6	15.6
	140.0	7.1	0.6
CO_2	115.3	4.2	1.8
	126.4	9.9	2.1
N_2	115.1	1.06	0.79
	116.7	1.06	1.47
	118.4	1.06	1.69
	120.6	1.06	2.78
	122.6	1.06	1.12
	123.0	1.59	0.26
	124.7	0.74	2.92
	125.2	1.59	0.37
	127.0	0.74	2.34
	127.6	0.94	1.09
	129.4	0.71	2.20
	130.2	0.71	2.20
	131.9	0.71	0.64
	132.8	0.80	1.38
	134.6	1.06	0.26
	135.8	0.80	3.97
	137.4	2.12	0.19
	138.8	0.94	2.85
	142.2	0.80	2.96
	145.4	1.06	1.53
O_2	140.7	25.20	21.46
	161.0	23.55	4.01

3.1. Solid methane

The ground state of CH_4 is $\tilde{X}^1A_1$ and its bond energy is $E_b(H{-}CH_3) = 4.5$ eV (Okabe 1978).

Figure 1 shows the VUV-absorption cross section of CH_4 as a function of the wavelength and photon energy. The high absorption of CH_4 ice around and below 120 nm, and the absorption of MgF_2 in the same spectral region only allowed spectroscopic measurements starting from 120 nm instead of 113 nm. As in Wu et al. (2012), a broad absorption band extending to 137 nm (9.05 eV) and centered on 124 nm (10.0 eV) was observed. This feature is attributed to the $1t_2$–$3s$ (D_{2d}) Rydberg transition. We detected a small bump near 140 nm (8.85 eV), which was not observed by Wu et al. (2012) in the solid phase or by Lee et al. (2001) in the gas phase. This feature may be produced by the VUV-absorption of a photoproduct. This phenomenon is more intense in the case of CO_2 studied in detail in Sect. 3.2. CH_4 ice presents high absorption at Ly-α (121.6 nm) and almost no absorption at Lyman band system wavelengths (132−165 nm).

The average VUV-absorption cross section has a value of $5.7^{+0.5}_{-1.1} \times 10^{-18}$ cm^2 in the 120−150 nm (10.33−8.26 eV). The total integrated VUV-absorption cross section has a value of $2.0^{+0.1}_{-0.4} \times 10^{-16}$ cm^2 nm ($1.5^{+0.1}_{-0.3} \times 10^{-17}$ cm^2 eV) in the same spectral region. The VUV-absorption cross sections of CH_4 ice at 121.6 nm is $1.4^{+0.1}_{-0.3} \times 10^{-17}$ cm^2, that is, at the Ly-α position of atomic hydrogen and there is no observable VUV-absorption in the position of the molecular hydrogen emission bands at 157.8 and 160.8 nm. Gas-phase data from Lee et al. (2001) were used for comparison with our solid-phase data, see Fig. 1, following Wu et al. (2012). The solid CH_4 absorption is shifted to shorter wavelength with respect to the gas data. The VUV-absorption cross section of CH_4 in the gas phase has an average value of 8.2×10^{-18} cm^2 in the 120−150 nm range. CH_4 gas data were integrated in the same range, giving a value of 2.9×10^{-16} cm^2 nm (2.09×10^{-17} cm^2 eV), which is higher than the solid CH_4 value. The VUV-absorption cross section of CH_4 gas at 121.6 nm is 1.8×10^{-17} cm^2.

3.2. Solid carbon dioxide

The ground state and bond energy of CO_2 are $X^1\Sigma_g^+$ and E_b(O−CO) = 5.5 eV (Okabe 1978).

The VUV-absorption cross section of CO_2 as a function of the wavelength and photon energy is shown in Fig. 2. This spectrum is very different from those reported in Lu et al. (2008), Mason et al. (2006), and Monahan & Walker (1974). Mason et al. (2006) observed two broad bands centered on 8.8 and 9.9 eV assigned to the $^1\Delta_u \leftarrow ^1\Sigma_g^+$ and $^1\Pi_g \leftarrow ^1\Sigma_g^+$ transitions. Lu et al. (2008) and Monahan & Walker (1974) reported a broad band centered on 9.8 eV. These authors found a vibrational structure in this band with similar positions. The intense absorption feature in the 107−120 nm (11.53−10.33 eV) region reported by Lu et al. (2008) is partially observed in our data. Two broad bands in the 120−133 nm (10.33−9.32 eV) and 133−163 nm (9.32−7.60 eV) regions were also reported by Lu et al. (2008), which are observed in our spectrum as well. A vibrational structure was detected in the 120−133 nm band, see Fig. 2 inlet. This vibrational structure is very faint in our spectrum, but 5 out of the 12 bands reported by Mason et al. (2006) are observable, see Table 3. In the 133−167 nm wavelength range of Fig. 2, the spectrum presents a CO-like VUV-absorption. Indeed, the VUV-light cone of our MDHL source processes the entire volume of the CO_2 ice and efficiently leads to the formation of CO by photodissociation of CO_2 molecules. After 9 min, corresponding to the collection time of a spectrum, CO is present with a column density that is 22% of the deposited CO_2 column density, estimated from integration of the IR bands, data not shown. This is enough, for a molecule like CO with a VUV-absorption cross section seven times larger than CO_2, to appear in the VUV-spectrum of CO_2 ice. The measured VUV-spectrum therefore corresponds to a mixture of CO_2 and CO, but because of the interaction of CO molecules with the CO_2 ice matrix, the CO features are shifted to shorter wavelengths than those of pure CO ice reported, for instance, in Paper I. This is shown in Fig. 3. Table 4 summarizes the peak positions of the detected CO features in the CO_2 ice and those reported for pure CO gas and ice. The $\Delta\lambda$- column in Table 4 represents a redshift with respect to pure CO gas and $\Delta\lambda$+ represents a blueshift with respect to the pure CO ice. These shifts gradually increase at higher wavelengths. The Davydov splitting is not observed in the features of CO in a CO_2 matrix where the (2, 0) transition is the strongest (as in pure CO gas; see, e.g., Paper I) in contrast to the VUV-absorption spectrum of pure CO ice, where the (1, 0) transition dominates. The band positions of CO_2 are not significantly affected by the presence of CO because the broad band centered on 9.8 eV (126.5 nm) and the vibrational structure in the 124−129 nm range of CO_2 present no detectable perturbations compared with other works with a much lower CO_2 photoproduction during spectral acquisition, and the band positions also agree fairly well with Lu et al. (2008), Mason et al. (2006), and Monahan & Walker (1974). The resulting fit and Gaussians involved are displayed in Fig. 2 as a red dashed-dotted trace. The 142.5 nm (8.70 eV) band reported by Lu et al. (2008) was not

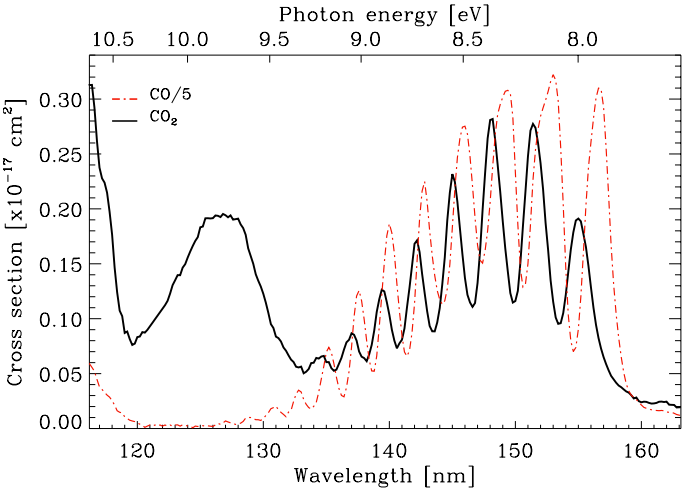

Fig. 3. Comparison between the VUV-absorption cross-section spectra of CO (red dashed-dotted trace) and CO_2 (black solid trace, the CO_2 ice is mixed with CO formed during the spectral acquisition). CO transitions in a CO_2 matrix are shifted to shorter wavelengths with respect to pure CO ice transitions.

Table 3. Transitions observed in the VUV-absorption cross-section spectrum of CO_2 ice in the 120−133 nm region.

This work		Mason et al. (2006)	Monahan & Walker (1974)
[nm]	[eV]	[eV]	[eV]
125.0	9.91	9.93	9.90
126.4	9.82	9.85	9.82
126.8	9.77	9.77	9.74
127.4	9.73	9.70	9.67
128.0	9.68	9.62	9.59

Notes. The positions agree fairly well with Mason et al. (2006) and Monahan & Walker (1974).

Table 4. Transitions of pure CO in gas and ice phases, and in a CO_2 matrix with a CO abundance of 22%.

(v', v'')	Lu et al. (2005) Pure CO gas [nm]	This work CO in CO_2 matrix $\Delta\lambda$-	[nm]	$\Delta\lambda$+	Paper I Pure CO ice [nm]
7, 0	134.7	0.1	134.8	0.4	135.2
6, 0	136.9	0.1	137.0	0.6	137.6
5, 0	139.3	0.1	139.4	0.6	140.0
4, 0	142.1	0.1	142.2	0.6	142.8
3, 0	144.8	0.2	145.0	1.0	146.0
2, 0	147.9	0.3	148.2	1.2	149.4
1, 0	151.1	0.3	151.4	1.6	153.0
0, 0	154.4	0.6	155.0	1.6	156.6

Notes. CO gas transitions are shifted to shorter wavelengths with respect to CO in a CO_2 matrix (column $\Delta\lambda$-), which in turn are shifted to shorter wavelengths with respect to pure CO ice transitions (column $\Delta\lambda$+).

Table 5. Transitions observed in the VUV-absorption cross-section spectrum of N_2. Columns (1) and (2) values are represented in Fig. 4.

(v', v'') (1) (2)	Position [nm]	[eV]	Area [cm^2 nm]	[cm^2 eV]
11, 0	115.2	10.76	7.0×10^{-22}	8.1×10^{-23}
10, 0	116.6	10.63	2.7×10^{-21}	2.5×10^{-22}
10, 0+9, 0	118.4	10.47	1.1×10^{-20}	1.0×10^{-21}
9, 0+8, 0	120.6	10.28	2.2×10^{-20}	1.9×10^{-21}
8, 0+7, 0	122.6	10.11	9.0×10^{-21}	6.8×10^{-22}
7, 0+6, 0	124.8	9.93	1.9×10^{-20}	1.6×10^{-21}
6, 0+5, 0	127.0	9.76	2.5×10^{-20}	1.9×10^{-21}
5, 0+4, 0	129.4	9.58	2.6×10^{-20}	1.9×10^{-21}
4, 0+3, 0	133.0	9.32	1.6×10^{-20}	1.2×10^{-21}
3, 0+2, 0	135.8	9.12	2.3×10^{-20}	1.6×10^{-21}
2, 0+1, 0	138.8	8.93	2.2×10^{-20}	1.5×10^{-21}
1, 0+0, 0	142.2	8.71	2.0×10^{-20}	1.2×10^{-21}
0, 0	145.4	8.52	1.2×10^{-20}	7.2×10^{-22}

fitted because of the overlap with the features of photoproduced CO in our experiment. The exact peak position of the feature at wavelengths shorter than 120 nm could not be confirmed because it is beyond our spectral range.

An upper limit for the average and the total integrated VUV-absorption cross section was calculated by subtracting CO, they are $6.7^{+0.5}_{-0.9} \times 10^{-19}$ cm^2 and $2.6^{+0.2}_{-0.3} \times 10^{-17}$ cm^2 nm ($1.9^{+0.1}_{-0.2} \times 10^{-18}$ cm^2 eV) in the wavelength range of 120−160 nm (10.33−7.74 eV). The VUV-absorption cross section of CO_2 ice at 121.6 nm is $1.0^{+0.1}_{-0.2} \times 10^{-18}$ cm^2. The VUV-absorption cross section at the Lyman band system range (132−165 nm) was not measured becuase of the presence of CO. Gas-phase data from Yoshino et al. (1996) were used for comparison with the solid phase data, see blue trace in Fig. 2. Mason et al. (2006) reported similar values for the gas- and solid-phase VUV-absorption cross sections, but using Yoshino et al. (1996) gas phase data, and our solid phase data we can clearly observe that the VUV-absorption cross section of CO_2 gas is lower than the solid-phase value, see Fig. 2. The Mason et al. (2006) solid-phase spectra displays a maximum at 9.9 eV with a VUV-absorption cross section of 1.2×10^{-18} cm^2, lower than the $1.9^{+0.1}_{-0.2} \times 10^{-18}$ cm^2 value deduced from our data. The VUV-absorption cross section of CO_2 in the gas-phase data from Yoshino et al. (1996) has an average value of 3.3×10^{-19} cm^2 120−160 nm range. CO_2 gas data were integrated in the spectral range, giving a value of 1.5×10^{-17} cm^2 nm (8.2×10^{-19} cm^2 eV), which is lower than the value for solid CO_2 in the same range ($2.6^{+0.2}_{-0.3} \times 10^{-17}$ cm^2 nm). The VUV-absorption cross section of CO_2 gas at 121.6 nm is very low, 6.3×10^{-20} cm^2.

It should be noted that, despite the photoproduced CO in our VUV-spectra of CO_2, the VUV-absorption cross sections are similar to previously reported values. The data presented in this section provide some evidence on the CO_2:CO mixture effects in the VUV-spectrum. The VUV-spectroscopy of ice mixtures has been poorly studied (Wu et al. 2012), but it is essential for understanding the absorption of UV-photons in icy grain mantles.

3.3. Solid nitrogen

The ground state and bond energy of N_2 are $X^1\Sigma_g^+$ and E_b(N−N) = 9.8 eV (Okabe 1978).

Owing to its very low VUV-absorption cross section, a deposition of 2.36 μm, nearly 4.7×10^{18} molecules cm^{-2}, for N_2 ice was required to detect the absorption features. The VUV-absorption cross section as a function of wavelength and photon energy is shown in Fig. 4. It presents a vibrational structure in the 114−147 nm (10.87−8.43 eV) region. Two systems (attributed to $a^1\Pi_g \leftarrow X^1\Sigma_g^+$ and $w^1\Delta_u \leftarrow X^1\Sigma_g^+$) can be observed. These systems have been reported by Boursey et al. (1978), Mason et al. (2006), and Wu et al. (2012). In agreement with Boursey et al. (1978) and Wu et al. (2012), we did not observe the two broad continua between 133−163 nm (9.30−7.60 eV) and 113−133 nm (9.30−11.0 eV) that Mason et al. (2006) reported. The VUV-absorption cross-section spectrum of N_2 is not as well resolved as in other works, but this probably does not affect the VUV-absorption cross-section scale we provide because no integration of the band area is involved. Table 5 summarizes the peak position and the band area integration of all the features presented. Even though our UV-lamp flux decreases below 120 nm, three features are observed in that spectrum range.

The average VUV-absorption cross section has a value of 7.0×10^{-21} cm^2 in the 114.6−146.8 nm (10.82−8.44 eV) range. The total integrated VUV-absorption cross section has a value of 2.3×10^{-19} cm^2 nm (1.8×10^{-20} cm^2 eV) in the same spectral region. The latter value is indeed affected by the low resolution of our VUV-absorption spectrum. A spectrum with better resolved bands would result in a lower value. Comparing our value of VUV-absorption cross section with data from Wu et al. (2012), we estimated an increase of 34% in the total integrated VUV-absorption cross-section value, therefore this integrated value would be $\sim 1.5 \times 10^{-19}$ cm^2 nm. The VUV-absorption cross section at Ly-α (121.6 nm) is very low; we estimated an upper limit value of 1.0×10^{-21} cm^2. There is no observable VUV-absorption at molecular hydrogen-band wavelengths (157.8 and 160.8 nm). Gas-phase VUV-absorption data adapted from Mason et al. (2006) are plotted in Fig. 4 as a blue dashed trace. The gas data of Mason et al. (2006) are not in cross section units, this is why we did not calculate the average and the total integrated VUV-absorption cross sections.

3.4. Solid oxygen

The ground state of O_2 is $X^3\Sigma_g^-$ and its bond energy is E_b(O−O) = 5.1 eV (Okabe 1978).

The VUV-absorption cross section as a function of wavelength and photon energy is shown in Fig. 5. The O_2 ice thickness estimation based on the fringes method, described in Sect. 3, requires a thick ice of about 60 ML. But the VUV-absorption cross-section measurement only works well for

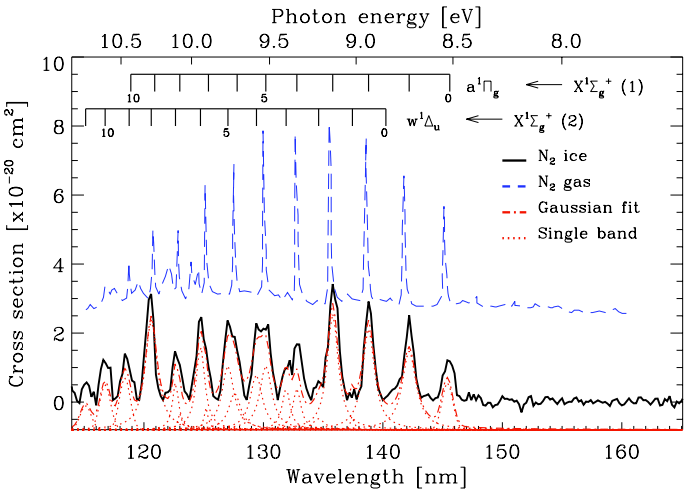

Fig. 4. VUV-absorption cross section as a function of photon wavelength (bottom X-axis) and VUV-photon energy (top X-axis) of N_2 ice deposited at 8 K, black solid trace. The blue dashed trace is the VUV-absorption cross-section spectrum of gas phase N_2 adapted from Mason et al. (2006). The fit, red dotted (single bands, see Table 2) and dashed-dotted trace, is the sum of twenty Gaussian profiles. It has been offset for clarity.

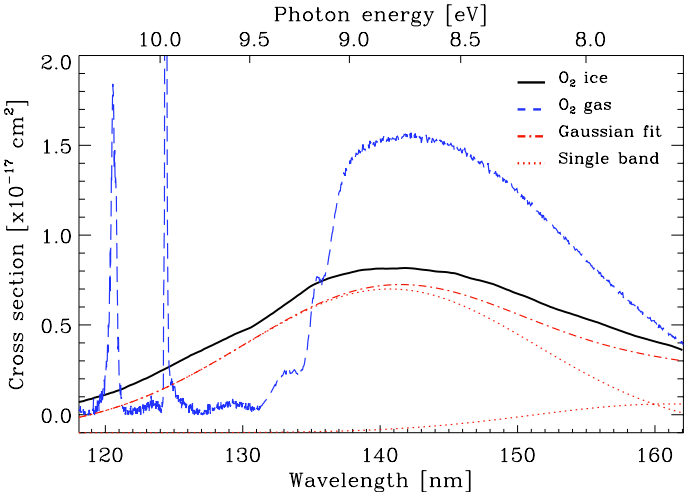

Fig. 5. VUV-absorption cross section as a function of photon wavelength (bottom X-axis) and VUV-photon energy (top X-axis) of O_2 ice deposited at 8 K, black solid trace. The blue dashed trace is the VUV-absorption cross-section spectrum of gas phase O_2 adapted from Lu et al. (2010). The fit, solid red dotted (single bands, see Table 2) and dashed-dotted trace, is the sum of two Gaussians. It has been offset for clarity.

thin ices below 200 ML. Therefore, several experiments were performed to ensure that the ice thickness estimation was correct in the case of O_2. Solid O_2 presents a broad band centered on 141 nm (8.79 eV) in the 118−162 nm (10.50−7.65 eV) region (attributed to the $\tilde{B}^3\Sigma_u^- \leftarrow X^3\Sigma_g^-$ transition, named Schumann-Runge band). It also presents a feature centered on 177 nm (7.0 eV), according to Mason et al. (2006) and Lu et al. (2008), which is beyond our spectral range. The resulting fit and Gaussians involved are represented in Fig. 5 by a red dashed-dotted trace. Following Lu et al. (2008), there is no obvious requirement for a broad line centered near 161 nm (7.70 eV), but without this band the resulting fit in the 150−162 nm range would not be as good.

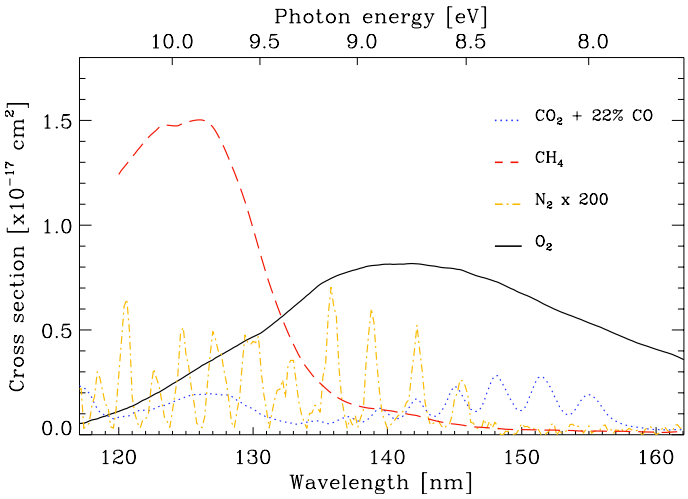

Fig. 6. VUV-absorption cross section as a function of wavelength (lower X-axis) and photon energy (top X-axis) of all the species in the solid phase at 8 K. The CO_2 absorption only occurs at wavelengths shorter than 133 nm, the absorption at longer wavelengths is due to the photo-produced CO during spectral adquisition.

The average VUV-absorption cross section has a value of $4.8^{+0.4}_{-1.0} \times 10^{-18}$ cm^2 in the 120−162 nm (10.33−7.65 eV) range. The total integrated VUV-absorption cross section has a value of $2.4^{+0.2}_{-0.5} \times 10^{-16}$ cm^2 nm ($1.5^{+0.1}_{-0.3} \times 10^{-17}$ cm^2 eV) in the same spectral region. The VUV-absorption cross sections of the O_2 ice at Ly-α (121.6 nm) and the molecular hydrogen band emissions (157.8 and 160.8 nm) are $1.4^{+0.1}_{-0.3} \times 10^{-18}$ cm^2, $4.6^{+0.4}_{-0.9} \times 10^{-18}$ cm^2, and $3.9^{+0.3}_{-0.8} \times 10^{-18}$ cm^2. Gas-phase data from Lu et al. (2010) were used for comparison with our solid phase data, see Fig. 5. Solid- and gas-phase data have a broad absorption band, but only the gas-phase spectrum presents discrete transitions. The VUV-absorption cross section of O_2 in the gas phase has an average value of 4.0×10^{-18} cm^2. The O_2 gas spectrum was integrated in the 118−162 nm range, giving a value of 3.3×10^{-16} cm^2 nm (2.0×10^{-17} cm^2 eV), which is higher than the solid-O_2 value. The VUV-absorption cross sections of O_2 gas at 121.6 nm, 157.8 nm and 160.8 nm are 2.5×10^{-18} cm^2, 6.5×10^{-18} cm^2, and 4.7×10^{-18} cm^2, which is also higher than the solid-phase measurements, with the exception of the Ly-α wavelength (121.6 nm).

3.5. Comparison between all the species

Figure 6 shows a comparison of the VUV-absorption cross section for all the species represented in the same linear scale. Because of its low VUV-absorption cross section, the N_2 spectrum was multiplied by a factor of 200 for better appreciation. It can be observed that the most highly absorbing molecule around the hydrogen Ly-α (121.6 nm) position is CH_4. Solid O_2 is most highly absorbing around the Lyman band system. N_2 gives the lowest absorption in both cases. All the species absorb at the Ly-α wavelength, with the exception of N_2, for which an upper limit was given in Sect. 3.3. CH_4 and N_2 absorb VUV-photons with wavelengths lower than 150 nm, while O_2 absorbs throughout the scanned range. Table 6 compares the VUV-absorption cross sections of all the species in the gas and solid phase as well as an average VUV-absorption cross section in the 120.8−122.6 nm and 132−162 nm range normalized by the Ly-α and Lyman band system photon flux of our MDHL.

Table 6. Comparison between the VUV-absorption cross sections in the 120−160 nm range of all the species in the gas and solid phase.

	Species	Total Int. [$\times 10^{-16}$ cm^2 nm]	Avg.	Ly-α	LBS	121.6 nm [$\times 10^{-18}$ cm^2]	157.8 nm	160.8 nm
Solid phase	CH_4	$2.0^{+0.1}_{-0.4}$	$5.7^{+0.5}_{-1.1}$	15	1.5	$14^{+0.1}_{-0.3}$	–	–
	CO_2	$0.26^{+0.02}_{-0.03}$	$0.67^{+0.5}_{-0.9}$	1.0	3.6	$1.0^{+0.1}_{-0.2}$	–	–
	N_2	0.0023	0.007	0.003	0.001	0.001	–	–
	O_2	$2.4^{+0.2}_{-0.5}$	$4.8^{+0.4}_{-1.0}$	1.5	5.4	$1.4^{+0.1}_{-0.3}$	$4.6^{+0.4}_{-0.9}$	$3.9^{+0.3}_{-0.8}$
Gas phase	CO_2[a]	0.15	0.33	–	–	0.063	0.17	0.095
	CH_4[b]	2.9	8.2	–	–	18	–	–
	N_2[c]	–	–	–	–	–	–	–
	O_2[d]	3.3	4.0	–	–	2.5	6.5	4.7

Notes. Total Int. is the total integrated VUV-absorption cross section in this range, Avg. is the average VUV-absorption cross section. Ly-α and LBS are the average VUV-absorption cross sections in the 120.8−122.6 nm and 132−162 nm range normalized by the photon flux. The last three columns are the VUV-absorption cross sections at wavelengths 121.6 nm (corresponding to the maximum intensity of the Ly-α peak), 157.8 and 160.8 nm (main peaks of the Lyman band system). All the VUV-absorption cross-section values in the table need to be multiplied by 1×10^{-18} cm^2, as indicated below.

References. Raw data adapted from [(a)] Lee et al. (2001); [(b)] Yoshino et al. (1996); [(c)] Mason et al. (2006); and [(d)] Lu et al. (2010) were used to calculate the reported gas-phase values.

4. Astrophysical implications

Interstellar and circumstellar ice mantles are composed of several species such as H_2O, CO, NH_3, CO_2, CH_4, and CH_3OH (Mumma & Charnley 2011, and ref. therein). In some cases, these molecular ice components are mixed in the ice mantle.

The VUV-absorption cross-section spectrum of CO_2 presented in this work has the disadvantage of being mixed with the CO produced by the VUV-irradiation of the MDHL used to acquire the VUV-spectroscopy of the species. But on the other hand, our data show that a binary ice mixture containing CO_2 and CO can lead to a mixed VUV-absorption spectrum where mixture effects can be appreciated, using this new way of performing VUV-spectroscopy (cf. Wu et al. 2010, 2012), where the band profiles and positions are altered to some extent by mixture effects.

As is commonly observed for example in infrared spectra, multicomponent ice mantles most likely display VUV-absorption features that correspond to the various species, where CO is the most highly absorbing molecule in the VUV among the common ice components. VUV-irradiation of CO2 ice led to a 22% of CO with respect to the starting CO_2 column density. CH_3OH ice led to 16% of CO for the same UV-fluence, see Paper I. The two production rates are similar but only the VUV-absorption cross-section spectrum of CO_2 ice presents CO features. On the other hand, the average VUV-absorption cross section of CH_3OH ice is almost ten times larger than the average VUV-absorption cross section of CO_2 in the 133−160 nm range.

The VUV-spectrum of CO in a CO_2 ice matrix is different from that of pure CO ice, with shifted positions that occur halfway between the gas and solid CO values, see Table 4 and Fig. 3. Therefore, CO in a solid CO_2 matrix can be treated as a highly porous CO ice mantle. Infrared spectroscopy of CO_2:CO = 20:1 ice shows a similar trend, the CO band shifts from 2138.6 cm^{-1} (for pure CO ice) to 2139.7 cm^{-1} and the FWHM increases from 2.5 cm^{-1} (pure CO ice) to 5.8 cm^{-1} (Sandford et al. 1988).

Formation of N_3 from N_2 irradiation with VUV-photons is extremely difficult (Hudson & Moore 2002). Proton and electron bombardment is more effective in the production of the azide radical than VUV-photons (Hudson & Moore 2002; Jamieson & Kaiser 2007). The likely explanation is the low VUV-absorption cross section of N_2. Detection of N_3 in space might be indicate a cosmic-ray field, or alternatively VUV-photons with energies higher than Ly-α (10.2 eV) that we were unable to study in this work. The latter possibility is very unlikely because much more intense absorption is not expected in the short interstellar radiation field range, from 91.2 to 114 nm, which was not measured in the laboratory.

Regarding the two homonuclear molecules studied, O_2 and N_2, the former presents a broad absorption band in the 118−160 nm range with a VUV-absorption cross section on the order of 10^{-18} cm^{-2}, while N_2 presents a vibrational structure in the 118−150 nm range with a VUV-absorption cross section on the order of 10^{-20} cm^{-2}. Using the Pontoppidan (2004) approximation of the abundances of nitrogen and oxygen, these two orders of magnitude differences can determine different photochemistry efficiencies for N_2 and O_2. This supports the hypothesis that a photochemistry richer in O than in N is expected in icy grain mantles, because a significant fraction of the N atoms might be locked as solid N_2.

The ice penetration depth of photons with a given wavelength, or the equivalent absorbing ice column density of a species in the solid phase, can be calculated from the VUV-absorption cross section following

$$N(\lambda) = \frac{-1}{\sigma(\lambda)} \ln\left(\frac{I_t(\lambda)}{I_0(\lambda)}\right), \quad (6)$$

which can be converted into an ice thickness using Eq. (3), inserting the volumetric density of the ice provided in Table 1:

$$d = \frac{N\, m_i}{N_A\, \rho_i}, \quad (7)$$

where $I_t(\lambda)$ is the transmitted intensity for a given wavelength λ, $I_0(\lambda)$ the incident intensity, $N(\lambda)$ is the absorbing column density in cm^{-2}, and $\sigma(\lambda)$ is the cross section in cm^2. Following the

Table 7. Column density of the different ice species corresponding to an absorbed photon flux of 95% and 99%.

Species	95% photon absorption			99% photon absorption		
	Ly-α	Avg.	Max.	Ly-α	Avg.	Max.
	($\times 10^{17}$ molec./cm^2)			($\times 10^{17}$ molec/cm^2)		
CH_4	2.1	5.3	1.8	3.3	8.1	2.7
CO_2	29.3	44.5	15.1	45.1	68.4	23.3
N_2	29957	4280	881	46052	6579	1354
O_2	21.4	6.2	3.7	32.9	9.6	5.6

Notes. Ly-α corresponds to the cross section at the Ly-α wavelength, 121.6 nm; in the case of N_2, the upper limit in the cross section leads to a lower limit in the absorbing column density. Avg. corresponds to the average cross section in the 120−160 nm range. Max. corresponds to the maximum cross section in the same wavelength range.

Table 8. VUV-absorption cross sections of O_2 ice for different photon energies.

Irrad. energy	σ	R^{inc}_{ph-des}	R^{abs}_{ph-des}
eV	l cm^2	molec/photon$_{inc}$	molec/photon$_{abs}$
10.5	7.1×10^{-19}	$\sim 1 \times 10^{-3}$	0.05
9.4	6.3×10^{-18}	$\sim 7 \times 10^{-3}$	0.04
8.6	8.0×10^{-18}	$\sim 4.5 \times 10^{-3}$	0.02
7.6	3.5×10^{-18}	$\sim 1.5 \times 10^{-3}$	0.015

Notes. R^{inc}_{ph-des} values were adapted from Fig. 3 of Fayolle et al. (2013) for the starting, maximum, and minimum photon energies (7.6, 9.4, and 10.5 eV). The 8.6 eV value was added because it also coincides with the average photon energy of our MDHL. The values in the table correspond to 30 ML of O_2 ice (i.e., a column density of 30×10^{15} molecules cm^{-2}), see Fayolle et al. (2013).

estimation for polar ice molecules provided in Paper I, Table 7 provides the column density values of nonpolar ice species that correspond to an absorbed flux of 95% and 99% using the cross-section value at Ly-α, the average cross section in the 120−160 nm range, and the maximum cross section in the same range.

Fayolle et al. (2013) reported the photodesorption of N_2 and O_2 ice as a function of photon wavelength, see Figs. 1 and 3 of that work. It can be observed that the photodesorption in the 10.8−8.4 eV spectral range is very low compared with the photodesorption in the 12.0−13.8 eV range for N_2. This is mainly due to the low absorption cross section that we report in that region, see Fig. 4. For O_2, Fig. 5 resembles the photodesorption profile of O_2 for different photon wavelengths in Fayolle et al. (2013).

Using the expression developed in Paper I,

$$R^{abs}_{ph-des} = \frac{I_0}{I_{abs}} R^{inc}_{ph-des}, \quad (8)$$

where I_0 and I_{abs} are the incident and the absorbed photon intensities at a certain wavelength, we can estimate the photodesorption rate per absorbed photon, R^{abs}_{ph-des}, which differs significantly from the photodesorption rate per incident photon, R^{inc}_{ph-des}, see Table 8.

For N_2 ice, Fayolle et al. (2013) reported an upper limit of $R^{inc}_{ph-des} \leq 4 \times 10^{-3}$ molecules per incident photon in the spectral range below 12.4 eV for $N = 30$ ML. The average absorption cross section for N_2 ice that we measured in that range is $\sigma = 7 \times 10^{-21}$ cm^2. The resulting photodesorption rate is quite high, $R^{abs}_{ph-des} \leq 19$ molecules per absorbed photon, meaning that a very small fraction of the incident photons are absorbed in the ice, but each absorbed photon led to the photodesorption of about 19 molecules on average (this in fact is a maximum value because Fayolle et al. (2013) measured photodesorption rates that *do not exceed* 4×10^{-3} molecules per incident photon).

A more direct comparison between N_2 and O_2 ice photodesorption rates could be made if the number of monolayers closer to the ice surface that truly contribute to the photodesorption were known. This value has not been estimated for other ices diferent from CO (about 5 ML, Muñoz Caro et al. 2010; Fayolle et al. 2011; and Chen et al. 2013). The above values of R^{inc}_{ph-des} and R^{abs}_{ph-des} correspond to the total ice column density of 30 ML in the experiment of Fayolle et al. (2013). With this uncertainty still remaining, we can conclude that when the VUV-absorption cross section of each specific ice composition is taken into account, it is possible to estimate the efficiency of the photodesorption per absorbed photon; in the case of N_2, for VUV photon energies that do not lead to direct dissociation of the molecules in the ice, these values are higher than unity. This observation and the fact that photons absorbed in ice monolayers deeper than the top monolayers (up to five for CO) can lead to a photodesorption event, indicate that the excess photon energy is transmitted to neighboring molecules in the ice within a certain range (Rakhovskaia et al. 1995; this range may correspond to about 5 ML in the case of CO ice, e.g. Muñoz Caro et al. 2010). In the case of O_2 the VUV photons have enough energy to dissociated the molecule, which makes it harder to measure the photodesorption rate because the dissociation dominates between the two processes.

5. Conclusions

This work adds to Paper I to complete our set of nine molecular ice components (CO, H_2O, CH_3OH, NH_3, H_2S, CH_4, CO_2, N_2, and O_2) selected to perform VUV-spectroscopy in the 120−160 nm spectral range. Some key aspects of this work are summarized below.

- For the first time, to our knowledge, the VUV-absorption cross sections of CH_4, N_2, and O_2 were measured for the solid phase, with average VUV-absorption cross sections of $5.7\ ^{+0.5}_{-1.1} \times 10^{-18}$ cm^2, $7.0\ ^{+0.6}_{-1.4} \times 10^{-21}$ cm^2, and $4.8\ ^{+0.4}_{-1.0} \times 10^{-18}$ cm^2. The total integrated VUV-absorption cross sections are $2.0\ ^{+0.1}_{-0.4} \times 10^{-16}$ cm^2 nm, $2.3\ ^{+0.2}_{-0.5} \times 10^{-19}$ cm^2 nm, and $2.4\ ^{+0.2}_{-0.5} \times 10^{-15}$ cm^2 nm. Our estimated value of the average VUV-absorption cross section of CO_2 ice, $2.6\ ^{+0.2}_{-0.3} \times 10^{-17}$ cm^2, is comparable with that reported by Mason et al. (2006), which was measured using a synchrotron as the monochromatic VUV-emission source.

- The ice samples made of N_2 or CO_2 display discrete VUV-absorption bands, the latter were not well resolved, while samples containing O_2 or CH_4 present a continuum VUV-absorption band, see Fig. 6, where N_2 presents by far the lowest VUV-absorption cross section.

- The ice sample is inevitably UV-irradiated for a few minutes during the spectral acquisition in our experimental configuration, which can lead to photoproduct formation. This effect is clearly observed in the case of CO_2 because the CO photoproduced has a large VUV-absorption cross section compared with CO_2 in the solid phase. In this experiment, the

CO bands are shifted in position and their profiles changed with respect to the pure CO ice spectrum reported in Paper I. These mixture effects were not significantly studied and have clear implications for the absorption of multicomponent ice mantles in space.

– The VUV-absorption cross sections of the two homonuclear molecules studied, N_2 and O_2, differ by two orders of magnitude. This affects their photodesorption rates and the formation of photoproducts in the ice matrix.

Acknowledgements. This research was financed by the Spanish MICINN under projects AYA2011-29375 and CONSOLIDER grant CSD2009-00038. This work was partially supported by NSC grants NSC99-2112-M-008-011-MY3 and NSC99-2923-M-008-011-MY3, and the NSF Planetary Astronomy Program under Grant AST-1108898.

References

Belloche, A., & André, P. 2003, ApJ, 593, 906
Bergin, E. A., Langer, W. D., & Goldsmith, P. F. 2002, ApJ, 570, L101
Boursey, E., Chandrasekharan, V., Gürtler, P., et al. 1978, Phys. Rev. Lett., 41, 1516
Brith, M., & Schnepp, O. 1965, Mol. Phys., 9, 473
Chen, Y.-J., Chu, C.-C., Lin, Y.-C., et al. 2010, Adv. Geosci., 25, 259
Chen, Y.-J., Chuang, K.-Y., & Muñoz Caro, G. M. 2013, ApJ, in press
Cheng, B.-M., Lu, H.-C., Chen, H.-K., et al. 2006, ApJ, 647, 1535
Cheng, B.-M., Chen, H.-F., Lu, H.-C., et al. 2011, ApJS, 196, 3
Chiar, J. E., Adamson, A. J., Kerr, T. H., & Whittet, D. C. B. 1995, ApJ, 455, 234
Collings, M. P., Anderson, M. A., Chen, R., et al. 2004, MNRAS, 354, 1133
Cruz-Diaz, G. A., Muñoz Caro, G. M., Chen, Y.-J., & Yih, T.-S. 2014, A&A, 562, A119 (Paper I)
Dalgarno, A., & Stephens, T. L. 1970, ApJ, 160, L107
Darwent, B. de B. 1970, National standard reference data system, 31, 70
Dawes, A., Mukerji, R. J., Davis, M. P., Holtom, P. D., & Webb, S. M. 2007, J. Chem. Phys., 126, 244711
Ehrenfreund, P., & van Dishoeck, E. F. 1998, Adv. Space Res., 21, 15
Feng, R., Cooper, G., & Brion, C. E. 1999, Chem. Phys., 244, 127
Fuchs, G. W., Acharyya, K., Bisschop, S. E., et al. 2006, Faraday Discussions, 133, 331
Fulvio, D., Sivaraman, B., Baratta, G. A., Palumbo, M. E., & Mason, N. J. 2009, Spectrochimica Acta Part A, 72, 1007
Gallo, A. R., & Innes, K. K. 1975, J. Mol. Spectrosc., 54, 472
Gerakines, P. A., Schutte, W. A., & Ehrenfreund, P. 1996, A&A, 312, 289
Goldsmith, P. F., Liseau, R., Bell, T. A., et al. 2011, ApJ, 737, 96
Gredel, R., Lepp, S., & Dalgarno, A. 1989, ApJ, 347, 289
Fayolle, E. C., Bertin, M., Romanzin, C., et al. 2011, ApJ, 739, L36
Fayolle, E. C., Bertin, M., Romanzin, C., et al. 2013, A&A, 556, A122
Hincelin, U., Wakelam, V., Hersant, F., et al. 2011, A&A, 530, A61
Hudson, R. D., & Carter, V. L. 1968, J. Opt. Soc. Am., 58, 227
Hudson, R. L., & Moore, M. H. 2002, ApJ, 568, 1095
Inn, E. C. Y. 1954, Spectrochimica Acta, 7, 65
Jamieson, C. S., & Kaiser, R. I. 2007, Chem. Phys. Lett., 440, 98
Jiménez-Escobar, A., & Muñoz Caro, G. M. 2011, A&A, 536, A11
Kuo, Y.-P., Lu, H.-C., Wu, Y.-J., Cheng, B.-M., & Ogilvie, J. F. 2007, Chem. Phys. Lett., 447, 168
Lee, A. Y. T., Yung, Y. L., Cheng, B.-M., et al. 2001, ApJ, 551, L93
Liseau, R., Goldsmith, P. F., Larsson, B., Pagani, L., & Bergman, P. 2012, A&A, 541, A73
Lu, H.-C., Chen, H.-K., Cheng, B.-M., Kuo, Y.-P., & Ogilvie, J. F. 2005, J. Phys. B: At. Mol. Opt. Phys., 38, 3693
Lu, H.-C., Chen, H.-K., Cheng, B.-M., & Ogilvie, J. F. 2008, Spectrochimica Acta Part A, 71, 1485
Lu, H. -C., Chen, H. -K., Chen, H. -F., Cheng, B.-M., & Ogilvie, J. F. 2010, A&A, 520, A19
Kalvans, J., & Shmeld, I. 2010, A&A, 521, A37
Mason, N. J., Dawes, A., Holton, P. D., et al. 2006, Faraday Discussions, 133, 311
Merrill, K. M., Russell, R. W., & Soifer, B. T. 1976, ApJ, 251, 533
Meyer, D. M., Jura, M., & Cardelli, J. A. 1998, ApJ, 493, 222
Monahan, K. M., & Walker, W. C. 1974, J. Chem. Phys., 61, 3886
Mota, R., Parafita, R., Giuliani, A., et al. 2005, Chem. Phys. Lett., 416, 152
Mumma, M. J., & Charnley, S. B. 2011, ARA&A, 49, 471
Muñoz Caro, G. M., Jiménez-Escobar, A., Martín-Gago, J. Á., et al. 2010, A&A, 522, A108
Nee, J. B., Suto, M., & Lee, L. C. 1985, Chem. Phys., 98, 147
Öberg, K. I., Fuchs, G. W., Awad, Z., et al. 2007, ApJ, 662, L23
Öberg, K. I., van Dishoeck, E. F., & Linnartz, H. 2009, A&A, 496, 281
Öberg, K. I., Boogert, A. C. A., Pontoppidan, K. M., et al. 2011, The Molecular Universe, Proc. IAU Symp., 280
Okabe, H. 1978, Photochemistry of small molecules (New York: John Wiley & Sons)
Pontoppidan, K. M., van Dishoeck, E. F., & Dartois, E. 2004, A&A, 426, 925
Pontoppidan, K. M., Blake, G. A., van Dishoeck, E. F., et al. 2008, ApJ, 684, 1323
Price, W. C., & Simpson, D. M. 1938, Proc. Roy. Soc. (Lond.), 165, 272
Rakhovskaia, O., Wiethoff, P., & Feulner, P. 1995, NIM B, 101, 169
Samson, J. A. R., & Ederer, D. L. 2000, Vacuum Ultaviolet Spectroscopy (Elsevier Inc)
Sandford, S. A., Allamandola, L. J., & Bernstein, M. P. 1997, From stardust to planetesimals, ASP Conf. Ser., 122, 201
Sandford, S. A., Allamandola, L. J., Tielens, A. G. G. M., & Valero, G. J. 1988, ApJ, 329, 498
Satorre, M. Á., Domingo, M., Millán, C., et al. 2008, Planet. Space Sci., 56, 1748
Smith, P. L., Rufus, L., Yoshino, K., & Parkinson, W. H. 2002, NASA Laboratory Astrophysics Workshop, NASA/CP-2002-21186, 158
Soifer, B. T., Puetter, R. C., Russell, R. W., et al. 1979, ApJ, 232, L53
Sternberg, A. 1989, ApJ, 347, 863
Tielens, A. G. G. M., Allamandola, L. J., Bregman, J., et al. 1984, ApJ, 287, 697
Tielens, A. G. G. M., Tokunaga, A. T., Geballe, T. R., & Baas, F. 1991, ApJ, 691, 1459
van Dishoeck, E. F., Phillips, T. G., Keene, J., & Blake, G. A. 1992, ApJ, 441, L222
Whittet, D. C. B., Schutte, W. A., Tielens, A. G. G. M., et al. 1996, A&A, 315, L357
Wu, Y.-J., Lu, H.-C., Chen, H.-K., & Cheng, B.-M. 2007, J. Chem. Phys., 127, 154311
Wu, Y.-J., Lin, M.-Y., Chou S.-L., et al. 2010, ApJ, 721, 856
Wu, Y.-J., Wu, C. Y. R., Chou S.-L., et al. 2012, ApJ, 746, 175
Yoshino, K., Esmond, J. R., Sun, Y., et al. 1996, J. Quant. Spectrosc. Radiat. Trans., 55, 53
Yamada, H., & Person, W. B. 1964, J. Chem. Phys., 41, 2478